NASA-TM-87627 19860012043

NASA Technical Memorandum 87627

Integration Effects of Underwing Forward- and Rearward-Mounted Separate-Flow, Flow-Through Nacelles on a High-Wing Transport

Milton Lamb and William K. Abeyounis

APRIL 1986

LIBRARY COPY

LANGLEY RESEARCH CENTER
LIBRARY, NASA
HAMPTON, VIRGINIA

NASA

NASA Technical Memorandum 87627

Integration Effects of Underwing Forward- and Rearward-Mounted Separate-Flow, Flow-Through Nacelles on a High-Wing Transport

Milton Lamb and William K. Abeyounis
Langley Research Center
Hampton, Virginia

National Aeronautics
and Space Administration

Scientific and Technical
Information Branch

1986

Introduction

Nacelle/pylon/wing integration has a decided effect on the aerodynamic performance of transonic transports. Previous studies (ref. 1) have shown the difficulty of reducing interference drag for conventional underwing pylon-mounted nacelles in a forward location. However, it has been shown theoretically that a lower installation drag may be obtained by placing the nacelles in the underwing, rearward-mounted location (ref. 2). An experimental investigation of a mixed-flow, flow-through nacelle mounted in the rearward underwing location was conducted in the Langley 16-Foot Transonic Tunnel (ref. 3). It was shown in reference 3 that the rearward-mounted nacelle had approximately one-half the combined value of form, wave, and interference drag (referred to as "interference plus form drag") of a comparable forward-mounted nacelle (ref. 4). Unpublished results show that favorable interference can be obtained for the rearward-mounted mixed-flow nacelle of reference 3. The present experimental investigation compared the longitudinal aerodynamic characteristics of configurations with pylon-mounted, separate-flow, flow-through nacelles in forward and rearward underwing locations. The effects of toe-in angle of the rearward-mounted nacelle/pylon were also investigated.

This investigation was conducted in the Langley 16-Foot Transonic Tunnel. Data were obtained for a free-stream Mach number range from 0.70 to 0.82 and an angle-of-attack range from -2.5° to 4.0°. The design cruise conditions were a free-stream Mach number of 0.80 and a lift coefficient of 0.45.

Symbols and Abbreviations

BL	buttline of model (lateral dimension), in.
b	wing span, 63.121 in.
C_D	drag coefficient, Drag/$q_\infty S$
$C_{D,i}$	internal drag coefficient
ΔC_D	installed drag coefficient, $C_{D,\mathrm{WBNP}} - C_{D,\mathrm{WB}}$
C_L	lift coefficient, Lift/$q_\infty S$
C_m	pitching-moment coefficient, Pitching moment/$q_\infty \bar{c} S$
C_p	pressure coefficient, $(p - p_\infty)/q_\infty$
c	local chord measure in wing reference plane, in.
c	mean geometric chord, 9.107 in.
FS	fuselage station (axial dimension measured from model nose), in.
M	free-stream Mach number
NBL	nacelle buttline, in.
NS	nacelle station (axial dimension measured from nacelle lip), in.
NWL	nacelle waterline, in.
p	local static pressure, lb/in^2
p_∞	free-stream static pressure, lb/in^2
q_∞	free-stream dynamic pressure, lb/in^2
r	nacelle radius, in.
S	wing reference area, 529.59 in^2
WL	fuselage water line, in.
WRP	wing reference plane (fig. 1(a))
x	local axial dimension, in.
x_{LE}	axial distance from pylon leading edge for defining shape of leading-edge section (fig. 4(a)), in.
x_{TE}	axial distance from pylon trailing edge for defining shape of trailing-edge section (fig. 4(a)), in.
y	local lateral dimension, in.
y_3	lateral dimension (see view A in fig. 4), in.
z	local vertical dimension, in.
α	angle of attack, deg
δ	nacelle toe-in angle, deg
η	wing semispan location, $y\frac{b}{2}$
ϕ	circumferential angular measurements for nacelle orifice locations (fig. 3), deg

Model components:

B	body
N	nacelle
P	pylon
W	wing

Experimental Apparatus and Procedure

Wind Tunnel

The experimental investigation was conducted in the Langley 16-Foot Transonic Tunnel. This tunnel

is an atmospheric, transonic, single-return type of tunnel with continuous air exchange and is capable of operating at Mach numbers from 0.20 to 1.30. A detailed description of the tunnel is presented in references 5 and 6.

Model and Support System

The 1/24-scale model, representative of a wide-body transport, is shown in figure 1(a); and a photograph of the model with the nacelles installed in the rearward location is shown in figure 1(b). The model was mounted on a sting-supported, six-component, strain-gauge balance. It had a high wing with supercritical airfoil sections. Details of the fuselage, wing, and wing pressure orifice locations can be found in references 3 and 4. The forward and rearward nacelle/pylon locations are shown in figure 2. The separate-flow nacelle consisted of a fan cowl and a core cowl, which are shown in figure 3. Also given are the internal and external contours and static pressure orifice locations. The details of the pylons are shown in figure 4. In addition, details of the bifurcator and diverter (see the rearward-mounted nacelle/pylon in fig. 2(b)) are shown in figure 5.

Instrumentation and Data Reduction

The model aerodynamic force and moment data were obtained by an internally mounted, six-component strain-gauge balance. The model surface static pressures were measured by scanning, electrical, strain-gauge transducers located in the model nose to reduce the lag time required between data points. Sting cavity pressures were measured by individual, remotely located, strain-gauge transducers.

All wind-tunnel parameters and model data were recorded simultaneously on magnetic tape. Except for scanning valve pressures, averaged values were used to compute all parameters. The model angle of attack was computed by correcting the support strut angle both for sting deflections based on balance loads and for tunnel upflow determined from inverted model runs in a previous tunnel entry. Sting cavity pressures were used to correct the longitudinal balance components for pressure forces in the sting cavity.

Nacelle internal drag corrections were made by using internal static pressures to determine the mass flow for a one-dimensional flow calculation, and then by integrating the computed internal pressure and friction forces (ref. 7). The internal surfaces of the fan and core cowl, the external surface of the core cowl, and the crosshatched areas of the diverter and pylon shown in figure 2 were included in the internal skin-friction calculations. The internal drag corrections are shown in figure 6 for the forward- and rearward-mounted nacelles. There was a large variation of internal drag with angle of attack for the forward-mounted nacelle. The rearward-mounted nacelle had only a slight variation in internal drag with angle of attack. A close examination of the internal drag results indicated that the difference in drag was the result of the pressure acting on the external surface of the core cowl. For the forward nacelle/pylon, these pressures are influenced by the flow around the wing leading edge, which changes significantly with angle of attack. For the rearward nacelle/pylon, these pressures were essentially constant with angle of attack.

Skin-friction drag was calculated using the method of Frankl and Voishel (ref. 8) for compressible turbulent flow over a flat plate. The forces and moments were transferred to the model moment center, the quarter-chord point of the mean geometric chord on the model waterline 0.0.

Tests

This experimental wind-tunnel investigation was conducted in the Langley 16-Foot Transonic Tunnel at free-stream Mach numbers from 0.70 to 0.82 and Reynolds numbers from approximately 2.5×10^6 to 3.0×10^6, based on the mean geometric chord of the wing. The model angle of attack was varied from $-2.5°$ to $4.0°$. Boundary-layer transition on the model was fixed using a grit transition-strip procedure (ref. 9). A 0.1-in-wide strip of No. 100 carborundum grit was attached 1.0 in. behind the nose of the fuselage. Strips of No. 90 and No. 80 grit were applied on the upper and lower wing surfaces (see fig. 11 in ref. 3) in a rearward location in order to match the boundary-layer thickness at the trailing edge of the wing (ref. 10). A 0.1-in. strip of No. 120 grit was placed 0.375 in. rearward of the nacelle lip of the fan and core cowls on the external and internal surfaces.

Results and Discussion

Effect of Nacelle Location

The effects of longitudinal placement of the nacelle/pylon on the static longitudinal aerodynamic characteristics are shown in figure 7 over the Mach number range. The addition of the forward nacelle/pylon to the wing-body configuration resulted in an increase in drag and the usual loss in lift. Changing the nacelle/pylon to a rearward location and changing the nacelle toe-in angle δ slightly resulted in a small decrease in drag compared with that of the forward nacelle/pylon configuration. However, not only was the lift loss associated with the addition

of a conventional forward nacelle/pylon regained but a significant increase in lift over that of the basic wing-body configuration was obtained.

Wing chordwise pressure distributions at span stations inboard, outboard, and along the centerline ($\eta = 0.370$) of the nacelle/pylon are presented in figure 8. At the nacelle/pylon centerline, the pressure orifices on the wing lower surface are covered by the forward pylon. At $\eta = 0.370$ the orifices along the wing upper surface and the orifice at $x/c > 0.8$ on the wing lower surface were covered by the rearward pylon.

The installation of the nacelle in the forward location resulted in an increase in pressure coefficient on the wing lower surface at $x/c < 0.15$, and then a decrease in pressure coefficient from $x/c \approx 0.15$ to $x/c \approx 0.50$ at $\eta = 0.328$. Similar effects were noted for the forward nacelle/pylon at $\eta = 0.440$, but to a lesser degree and at slightly different x/c locations. The forward nacelle/pylon caused an initial decrease in pressure coefficient on the wing upper surface at $\eta = 0.328$; but at $\eta = 0.370$ and 0.440, the pressure coefficients were essentially unaffected.

The installation of the nacelle in a rearward location resulted in an increase in wing lower surface pressure coefficients extending from the nacelle inlet ($x/c \approx 0.70$) forward to near the leading edge of the wing at $\eta = 0.328$ and 0.370. With the nacelle in the rearward location beneath the wing, the nacelle inlet is similar to a trailing-edge flap. When the velocity is reduced (pressure coefficient increased) below the wing, there is an increase in lift that is the reverse of the results obtained for the nacelle located forward of the wing. The expected drag reduction was not obtained because of the decrease in pressure rearward of $x/c = 0.6$, as shown in the lower surface pressures of figure 8(c).

Effect of Nacelle/Pylon Toe-in Angle

The effects of nacelle/pylon toe-in angle on the longitudinal aerodynamic characteristics are shown in figure 9 at $M = 0.80$ for the rearward nacelle/pylon configuration. Increasing the toe-in angle of the nacelle/pylon from $-1.5°$ to $-2.6°$ resulted in an increase in drag in the lower lift range, but the drag polar was rotated (induced drag reduction) such that there was a decrease in drag above $C_L = 0.55$. There was essentially no difference in lift coefficients for the two toe-in angles. Again, the pressure coefficients are presented at $\eta = 0.328$, 0.370, and 0.440. (See fig. 10.) The only effect of toe-in angle on the pressures was to influence the wing upper surface pressures as the pylon moved toward or away from the pressure orifices.

Installed Drag

The installed drag coefficient

$$\Delta C_D = C_{D,\mathrm{WBNP}} - C_{D,\mathrm{WB}}$$

is presented in figure 11 for $M = 0.80$ and $C_L = 0.45$. The unshaded area indicates the amount of installed drag that may be attributed to calculated nacelle/pylon skin-friction drag. The shaded area represents the combined value of form, wave, and interference drag. The configuration with the nacelle/pylon installed in the rearward location had the lowest installed drag. When compared with the forward nacelle/pylon, the rearward-mounted configuration had a slightly higher interference plus form drag but a lower skin-friction drag because the rearward-pylon wetted area was approximately one-half that of the forward pylon. Changing the toe-in angle of the rearward nacelle/pylon from $-1.5°$ to $-2.6°$ resulted in a slightly higher installed drag. In all cases, the interference plus form drag was excessively high, based on the results of a similar test with mixed-flow nacelles (ref. 3).

Summary of Results

An experimental investigation has been conducted in the Langley 16-Foot Transonic Tunnel at free-stream Mach numbers from 0.70 to 0.82 and angles of attack from $-2.5°$ to $4.0°$ to determine the integration effects of pylon-mounted underwing forward and rearward separate-flow, flow-through nacelles on a high-wing transonic transport configuration. The results are summarized as follows:

1. At cruise, the configuration with the nacelle/pylon in a rearward location and with a toe-in angle of $-1.5°$ had the lowest installed drag. This lower drag was due to the reduction in calculated skin friction of the nacelle/pylon configuration.

2. In all cases the combined value of form, wave, and interference drag was excessively high.

3. The configuration with the necelle/pylon in a rearward location produced an increase in lift over that of the basic wing-body configuration.

NASA Langley Research Center
Hampton, VA 23665-5225
December 24, 1985

References

1. Henderson, William P.; and Patterson, James C., Jr.: Propulsion Installation Characteristics for Turbofan Transports. AIAA-83-0087, Jan. 1983.
2. Kuchemann, Dietrich; and Weber, Johanna: *Aerodynamics of Propulsion, First ed.* McGraw-Hill Book Co., Inc., 1953.
3. Abeyounis, William K.; and Patterson, James C., Jr.: *Effect of Underwing Aft-Mounted Nacelles on the Longitudinal Aerodynamic Characteristics of a High-Wing Transport Airplane.* NASA TP-2447, 1985.
4. Lee, Edwin E., Jr.; and Pendergraft, Odis C., Jr.: *Installation Effects of Long-Duct Pylon-Mounted Nacelles on a Twin-Jet Transport Model With Swept Supercritical Wing.* NASA TP-2457, 1985.
5. Corson, Blake W., Jr.; Runckel, Jack F.; and Igoe, William B.: *Calibration of the Langley 16-Foot Transonic Tunnel With Test Section Air Removal.* NASA TR R-423, 1974.
6. Peddrew, Kathryn H., compiler: *A User's Guide to the Langley 16-Foot Transonic Tunnel.* NASA TM-83186, 1981.
7. Putnam, Lawrence E.: *Effects of Upper-Surface Nacelles on Longitudinal Aerodynamic Characteristics of High-Wing Transport Configuration.* NASA TP-2579, 1986.
8. Shapiro, Ascher H.: *The Dynamics and Thermodynamics of Compressible Fluid Flow. Volume II.* Ronald Press Co., c.1954.
9. Braslow, Albert L.; Hicks, Raymond M.; and Harris, Roy V., Jr.: *Use of Grit-Type Boundary-Layer-Transition Trips on Wind-Tunnel Models.* NASA TN D-3579, 1966.
10. Blackwell, James A., Jr.: *Preliminary Study of Effects of Reynolds Number and Boundary-Layer Transition Location on Shock-Induced Separation.* NASA TN D-5003, 1969.

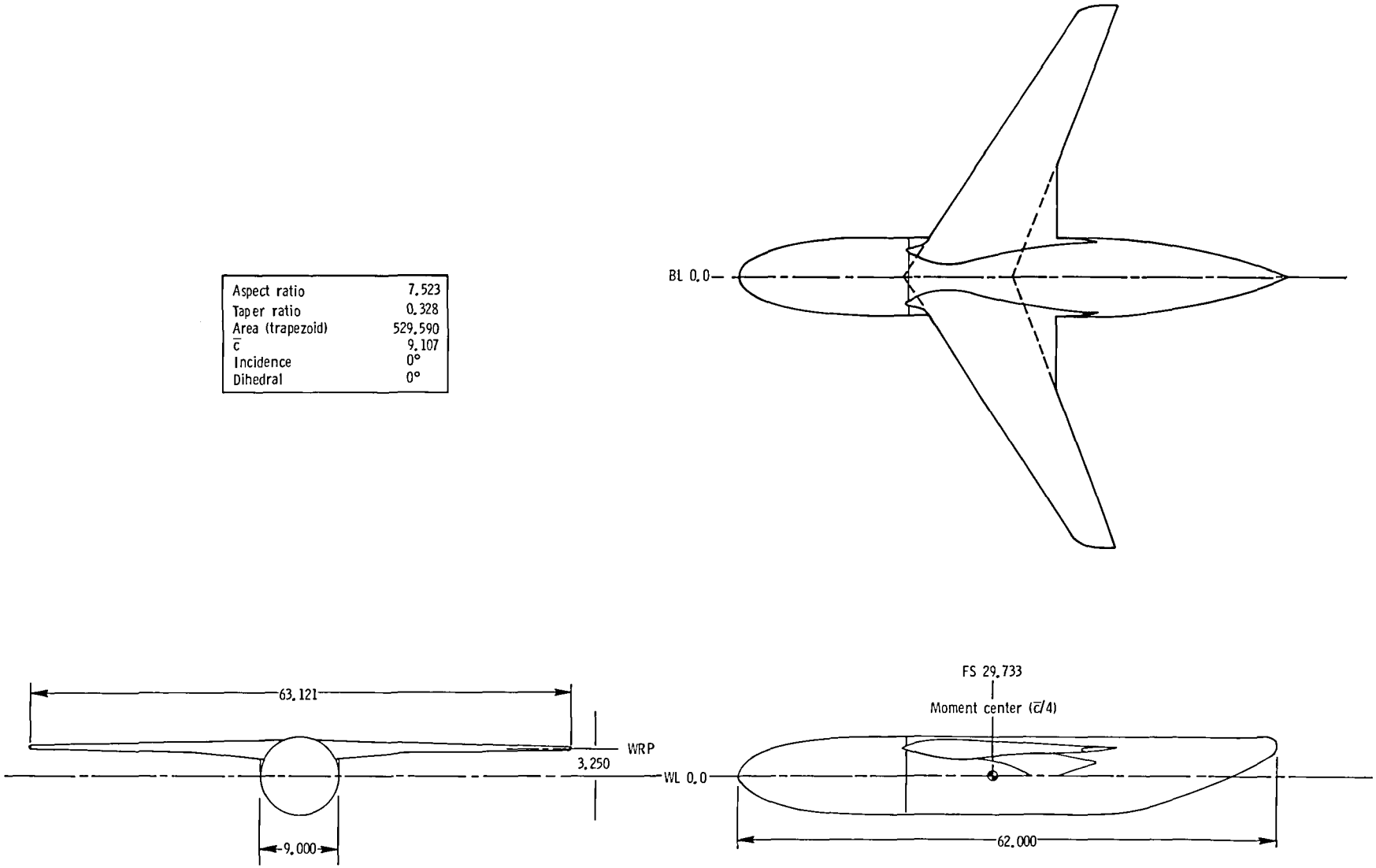

(a) General layout.

Figure 1. Details of model. All dimensions are in inches.

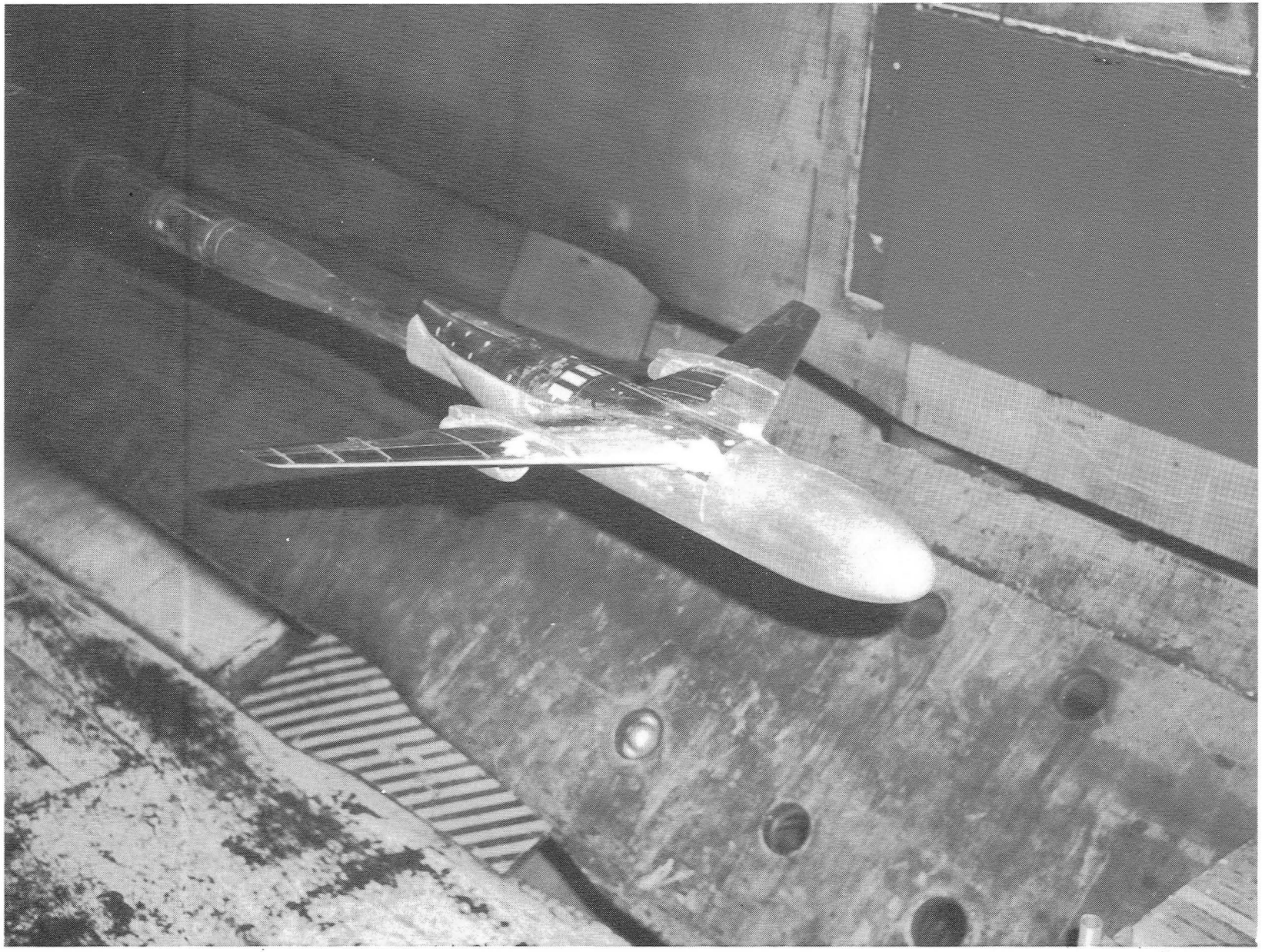

L-83-9666

(b) Model installed in the Langley 16-Foot Transonic Tunnel.

Figure 1. Concluded.

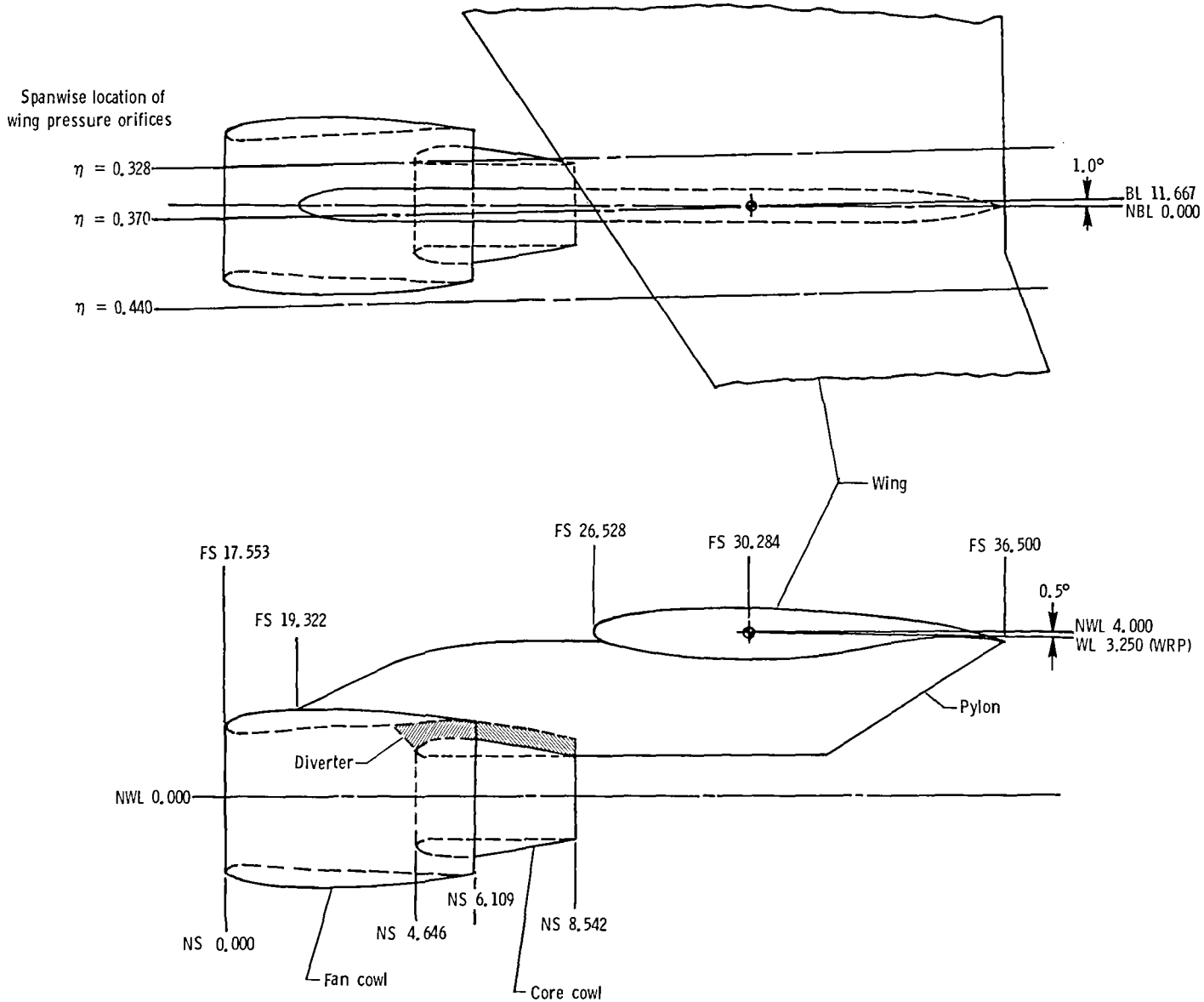

(a) Forward-mounted nacelle.

Figure 2. Nacelle/pylon locations. Linear dimensions are in inches.

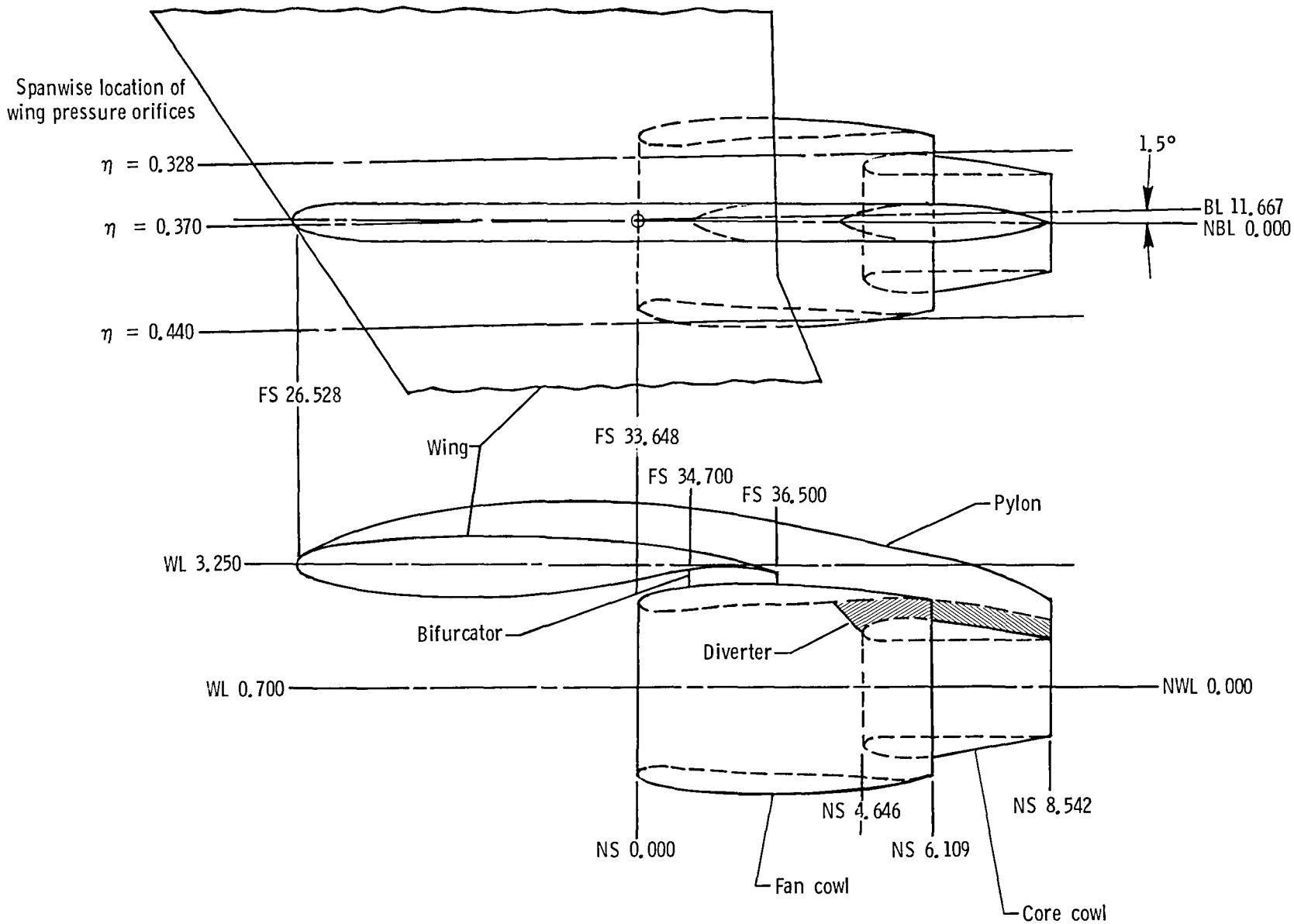

(b) Rearward-mounted nacelle.

Figure 2. Concluded.

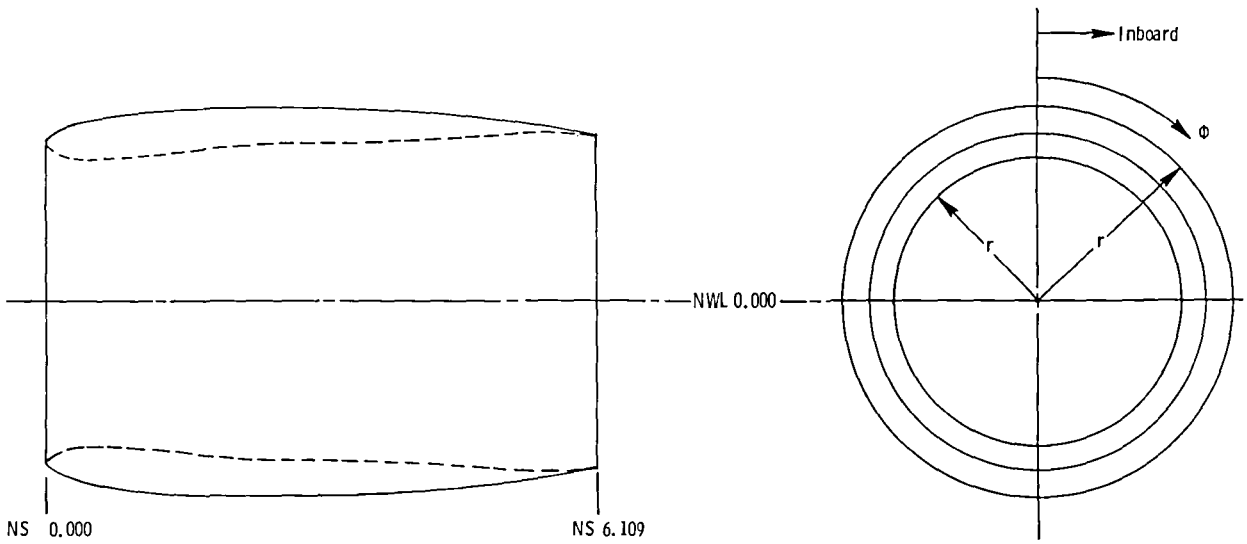

External contour			
NS	r	NS	r
0.000	1.769	2.616	2.132
0.001	1.779	2.917	2.131
0.002	1.784	3.105	2.129
0.023	1.827	3.292	2.125
0.112	1.884	3.443	2.122
0.206	1.924	3.630	2.115
0.262	1.943	3.818	2.107
0.374	1.975	3.968	2.099
0.505	2.005	4.156	2.087
0.674	2.037	4.344	2.073
0.786	2.055	4.532	2.055
0.898	2.070	4.644	2.043
1.085	2.092	4.720	2.035
1.235	2.106	4.832	2.022
1.348	2.114	4.907	2.012
1.535	2.124	5.020	1.996
1.610	2.127	5.095	1.985
1.797	2.131	6.109	1.831
1.871	2.132		

Internal contour			
NS	r	NS	r
0.000	1.769	2.867	1.749
0.002	1.753	3.015	1.750
0.005	1.741	3.164	1.752
0.095	1.651	3.387	1.757
0.178	1.617	3.610	1.764
0.214	1.607	3.758	1.769
0.286	1.593	3.981	1.778
0.327	1.589	4.130	1.786
0.397	1.586	4.279	1.794
0.547	1.587	4.502	1.808
0.697	1.593	4.725	1.823
0.847	1.601	4.948	1.841
1.146	1.627	5.171	1.861
1.446	1.658	5.283	1.872
1.745	1.690	5.358	1.877
2.045	1.719	5.433	1.880
2.344	1.740	5.508	1.880
2.494	1.746	5.583	1.877
2.644	1.748	5.658	1.871
2.718	1.748	6.109	1.818

	External pressure orifices at Φ of				
NS	30°	90°	180°	270°	330°
0.138	↓	↓	↓	↓	↓
0.288					
0.588					
0.851					
1.152					
1.640					
3.217					
4.719					
5.358	↓	↓	↓	↓	↓

Internal pressure orifices located at NS 2.875 for Φ of 0°, 90°, 180°, and 270°

(a) Fan cowl.

Figure 3. Details of separate-flow nacelles. Linear dimensions are in inches.

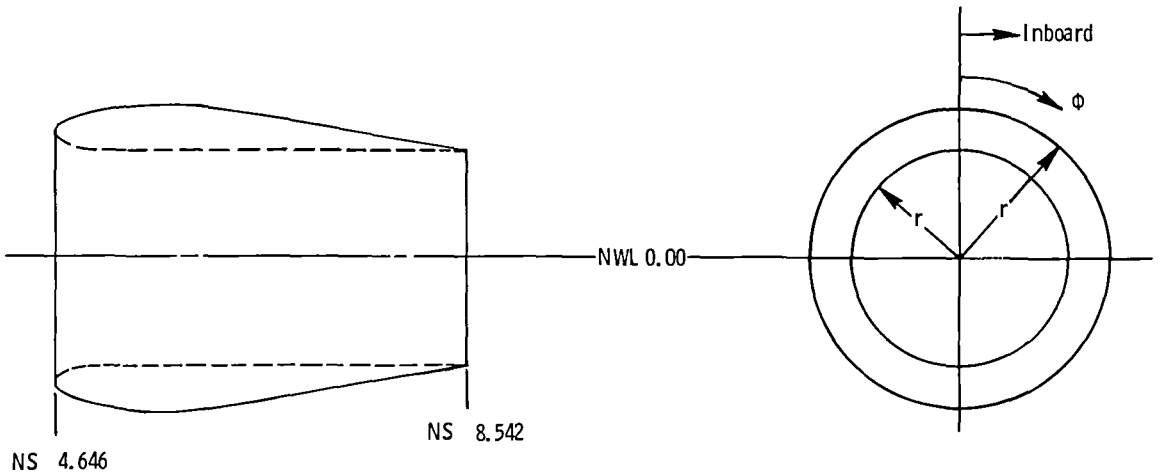

External contour			
NS	r	NS	r
4.646	1.168	5.229	1.398
4.648	1.184	5.273	1.404
4.668	1.218	5.318	1.410
4.685	1.233	5.363	1.415
4.702	1.246	5.408	1.419
4.736	1.266	5.453	1.423
4.747	1.272	5.497	1.427
4.769	1.283	5.542	1.429
4.803	1.297	5.587	1.434
4.825	1.305	5.632	1.434
4.870	1.320	5.676	1.435
4.915	1.334	5.744	1.436
4.949	1.343	5.771	1.437
5.005	1.357	5.846	1.433
5.083	1.373	5.884	1.430
5.139	1.384	5.921	1.426
5.184	1.391	5.949	1.421
5.206	1.394	8.542	0.996

Internal contour	
NS	r
4.646	1.168
4.649	1.147
4.655	1.134
4.663	1.120
4.674	1.107
4.695	1.088
4.723	1.070
4.755	1.054
4.792	1.039
4.833	1.026
4.877	1.015
4.941	1.004
4.991	0.999
5.043	0.996
5.078	0.996
8.542	0.996

	External pressure orifices at Φ of		
NS	30°	90°	180°
6.034	↓	↓	↓
6.785			
7.461			
8.174			

Internal pressure orifices located at NS 6.409 for Φ of 0°, 90°, 180°, and 270°

(b) Core cowl.

Figure 3. Concluded.

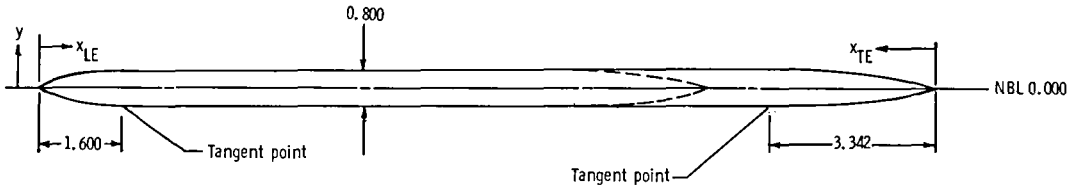

Pylon leading-edge section	
x_{LE}	y
0.000	0.000
0.020	0.060
0.030	0.073
0.050	0.091
0.100	0.124
0.200	0.173
0.300	0.211
0.400	0.243
0.600	0.294
0.800	0.332
1.000	0.361
1.200	0.382
1.400	0.395
1.600	0.400

Pylon trailing-edge section	
x_{TE}	y
0.000	0.008
0.501	0.072
1.003	0.129
1.504	0.200
2.005	0.282
2.507	0.334
2.841	0.375
3.108	0.393
3.342	0.400

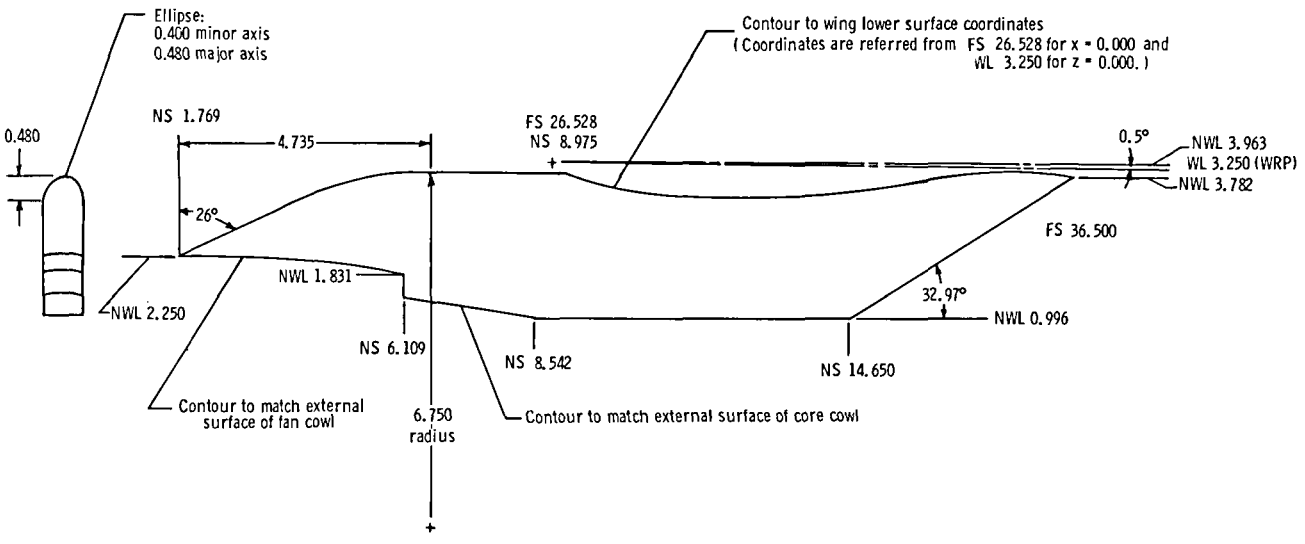

Lower-wing coordinates			
x	z	x	z
0.000	-0.038	3.490	-0.672
0.020	-0.099	3.989	-0.668
0.050	-0.137	4.488	-0.649
0.100	-0.179	4.986	-0.613
0.199	-0.234	5.485	-0.559
0.399	-0.308	5.983	-0.489
0.598	-0.365	6.482	-0.404
0.798	-0.412	6.981	-0.312
0.997	-0.453	7.479	-0.221
1.396	-0.519	7.978	-0.139
1.795	-0.573	8.477	-0.081
2.194	-0.613	8.975	-0.063
2.593	-0.642	9.972	-0.164
2.992	-0.661		

(a) Forward-mounted pylon.

Figure 4. Details of pylons. Linear dimensions are in inches.

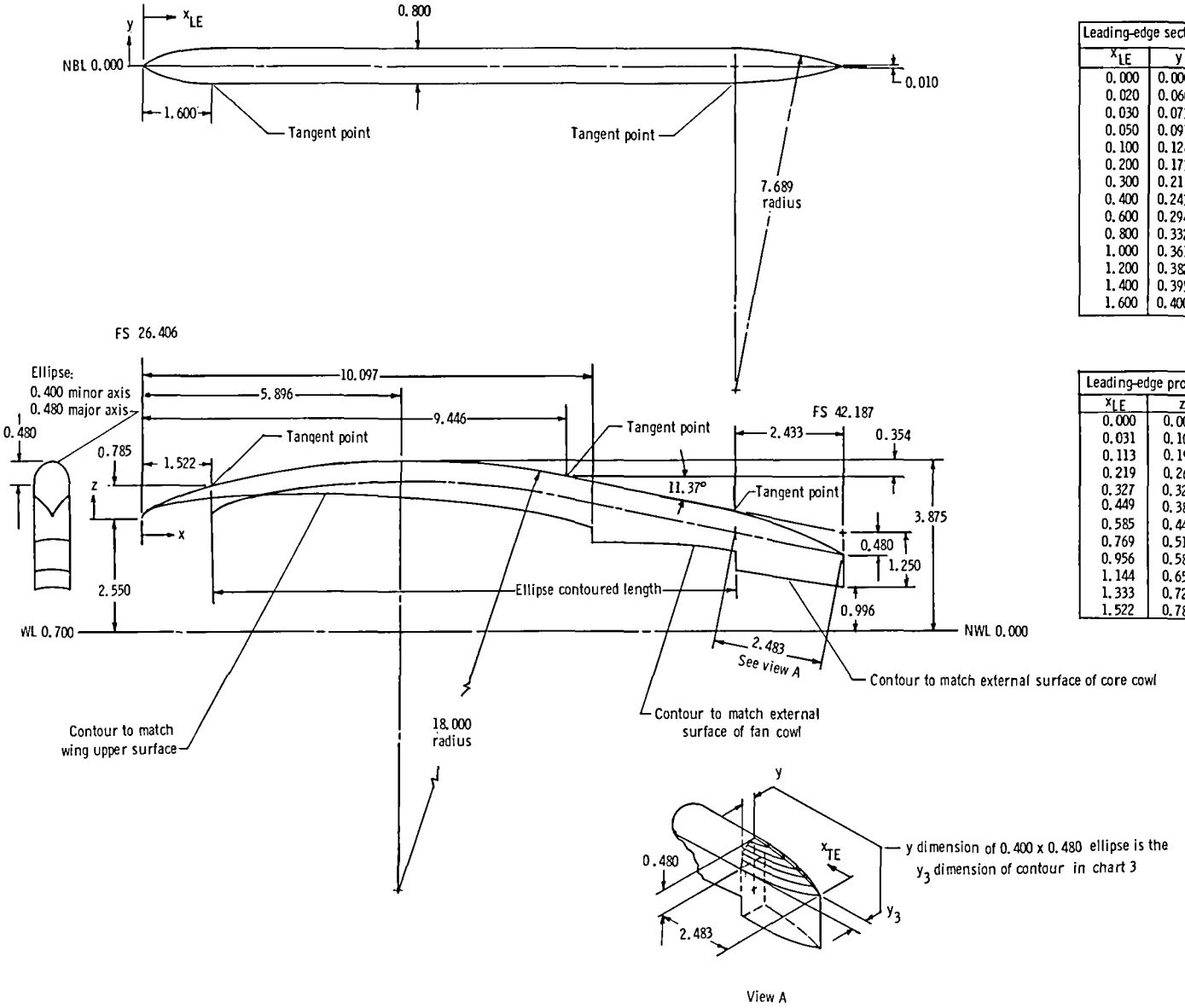

Leading-edge section	
x_{LE}	y
0.000	0.000
0.020	0.060
0.030	0.073
0.050	0.091
0.100	0.124
0.200	0.173
0.300	0.211
0.400	0.243
0.600	0.294
0.800	0.332
1.000	0.361
1.200	0.382
1.400	0.395
1.600	0.400

Leading-edge profile	
x_{LE}	z
0.000	0.000
0.031	0.100
0.113	0.192
0.219	0.268
0.327	0.329
0.449	0.388
0.585	0.446
0.769	0.519
0.956	0.589
1.144	0.656
1.333	0.721
1.522	0.785

Chart 3	
x_{TE}	y_3
0.000	0.000
0.000	0.005
0.049	0.021
0.102	0.038
0.204	0.069
0.306	0.098
0.510	0.153
0.638	0.184
0.765	0.214
0.893	0.241
1.021	0.265
1.148	0.288
1.276	0.308
1.403	0.327
1.531	0.343
1.658	0.357
1.786	0.370
1.913	0.380
2.041	0.388
2.169	0.394
2.296	0.398
2.359	0.399
2.483	0.400

(b) Rearward-mounted pylon.

Figure 4. Concluded.

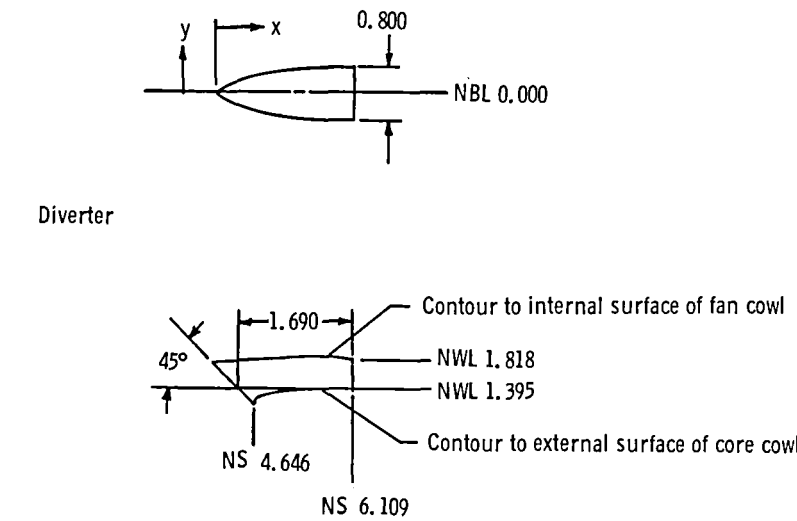

Diverter coordinates			
x	y	x	y
0.000	0.000	0.839	0.312
0.010	0.018	0.874	0.320
0.023	0.026	0.910	0.328
0.058	0.046	0.945	0.945
0.094	0.066	0.981	0.342
0.129	0.085	1.016	0.348
0.165	0.103	1.051	0.355
0.200	0.119	1.087	0.360
0.236	0.134	1.122	0.365
0.271	0.148	1.158	0.370
0.307	0.161	1.193	0.375
0.342	0.173	1.229	0.379
0.360	0.178	1.264	0.382
0.378	0.183	1.300	0.385
0.413	0.193	1.355	0.388
0.448	0.204	1.371	0.391
0.484	0.214	1.406	0.393
0.519	0.224	1.442	0.395
0.555	0.234	1.477	0.396
0.590	0.245	1.513	0.398
0.626	0.255	1.548	0.399
0.661	0.265	1.584	0.399
0.697	0.275	1.619	0.400
0.732	0.285	1.655	0.400
0.768	0.294	1.690	0.400
0.803	0.303		

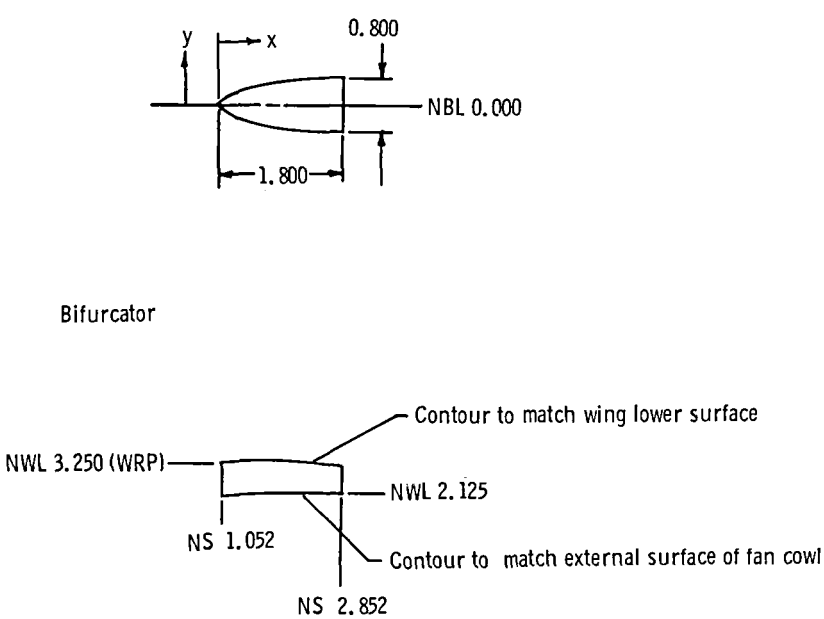

Bifurcator coordinates			
x	y	x	y
0.000	0.000	0.756	0.319
0.001	0.012	0.806	0.327
0.004	0.024	0.855	0.335
0.009	0.039	0.905	0.342
0.019	0.055	0.954	0.349
0.035	0.073	1.004	0.355
0.057	0.093	1.053	0.361
0.087	0.115	1.103	0.366
0.126	0.139	1.153	0.371
0.178	1.203	0.376	0.376
0.224	0.184	1.253	0.380
0.271	0.201	1.302	0.384
0.318	0.217	1.352	0.387
0.366	0.232	1.402	0.390
0.414	0.245	1.452	0.393
0.463	0.258	1.502	0.395
0.511	0.270	1.552	0.397
0.560	0.281	1.602	0.398
0.609	0.291	1.652	0.399
0.658	0.301	1.702	0.400
0.707	0.310	1.750	0.400

Figure 5. Details of bifurcator and diverter. Linear dimensions are in inches.

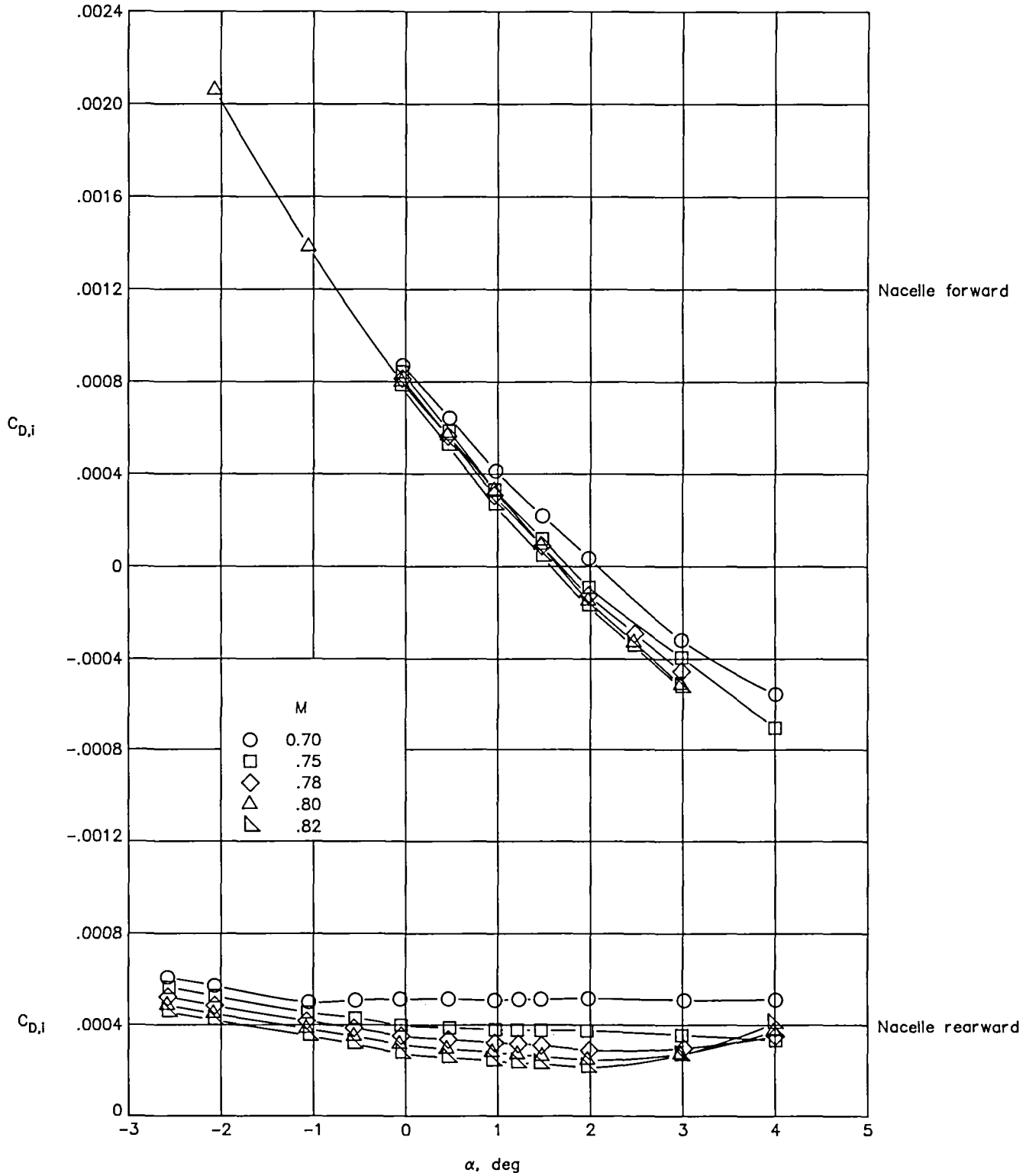

Figure 6. Nacelle internal drag corrections.

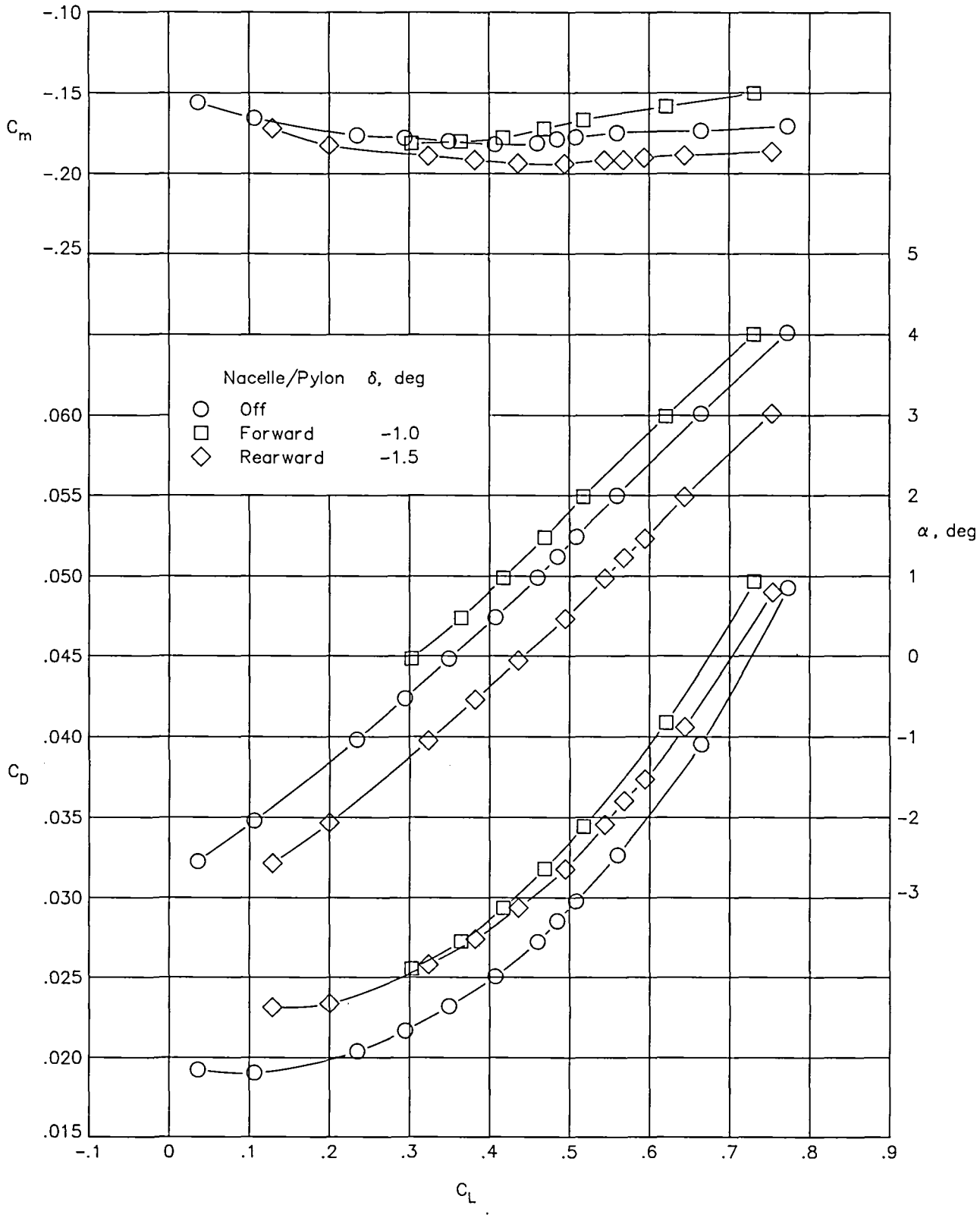

(a) $M = 0.70$.

Figure 7. Effects of nacelle/pylon longitudinal location on longitudinal aerodynamic characteristics.

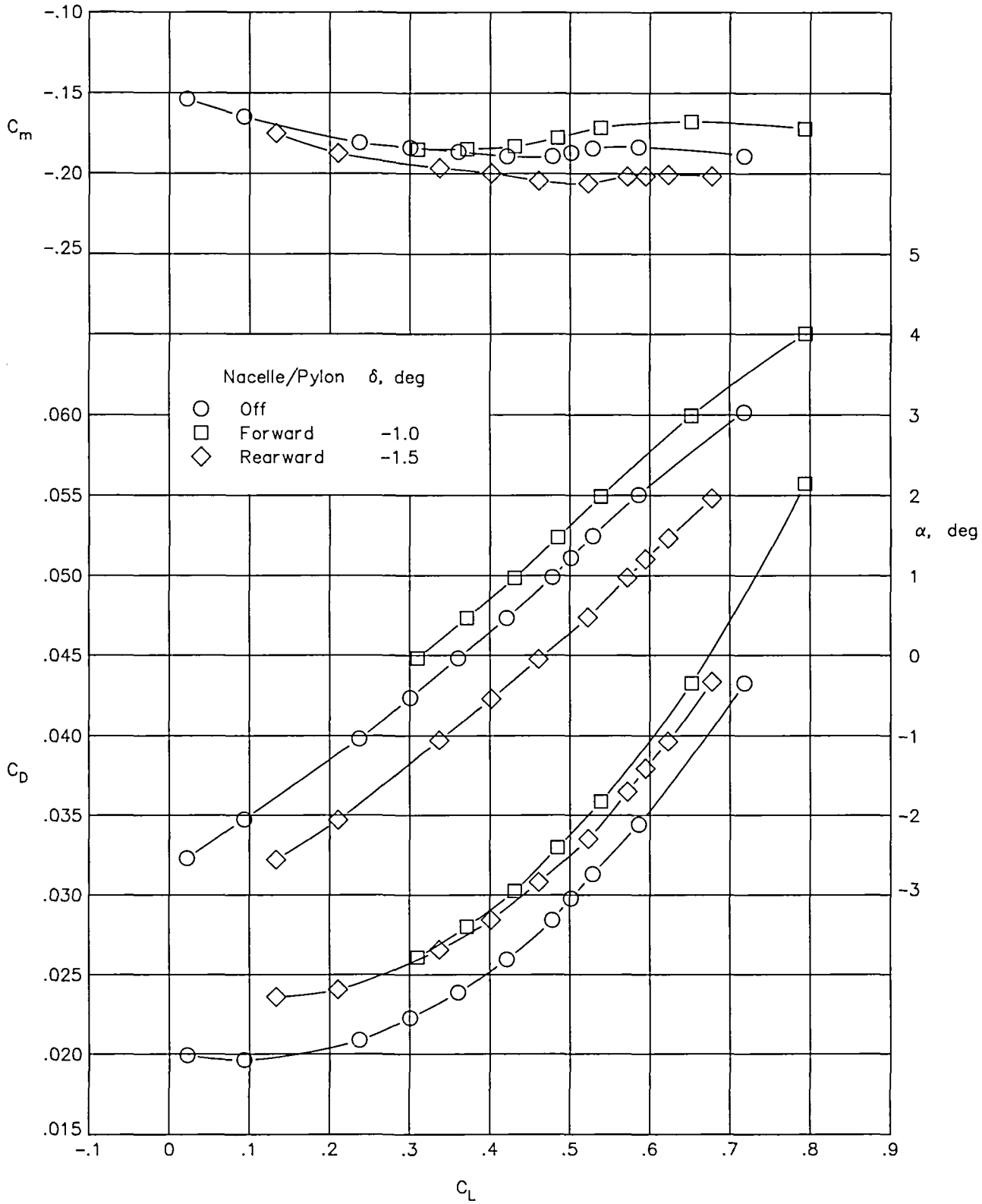

(b) $M = 0.75$.

Figure 7. Continued.

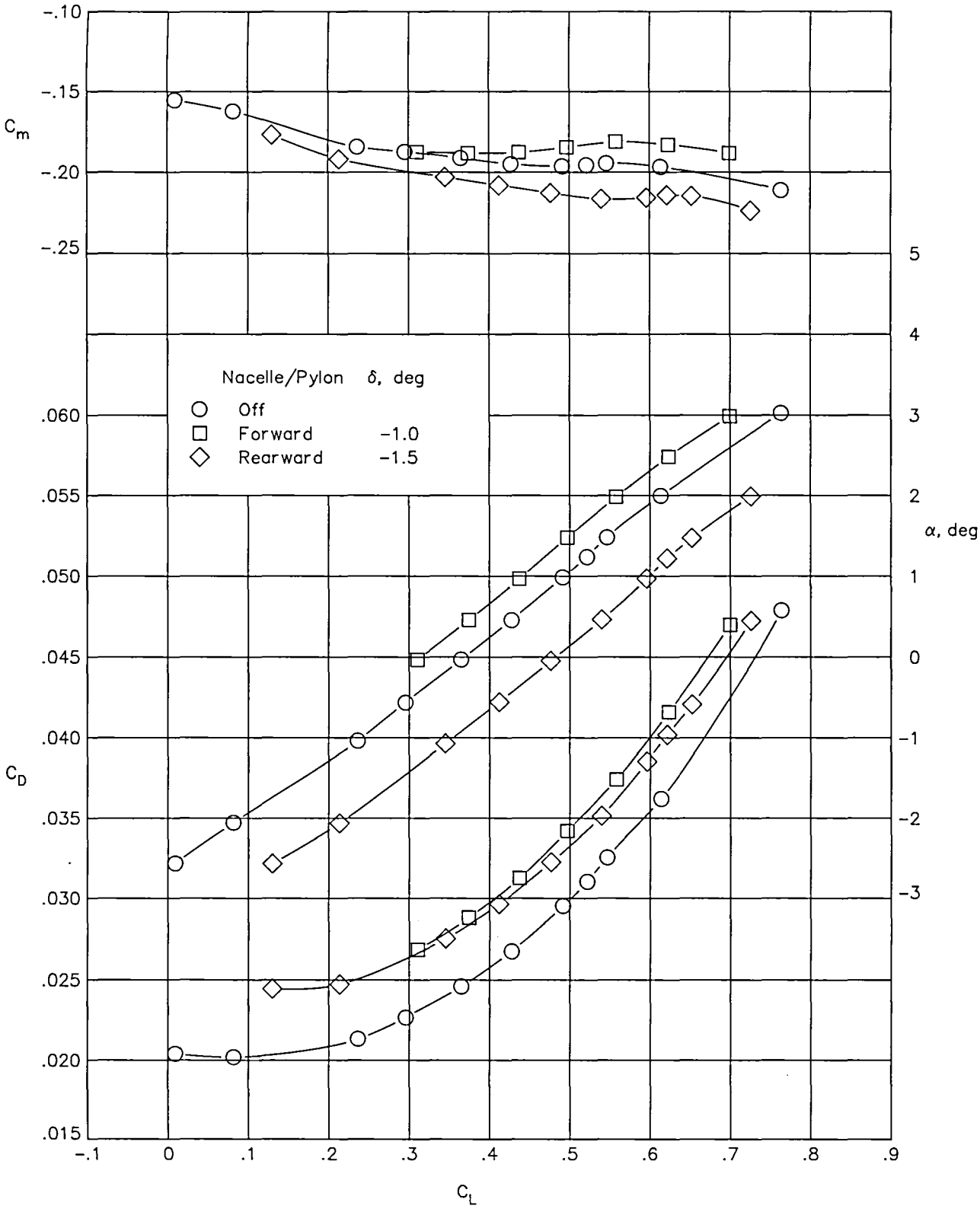

(c) $M = 0.78$.

Figure 7. Continued.

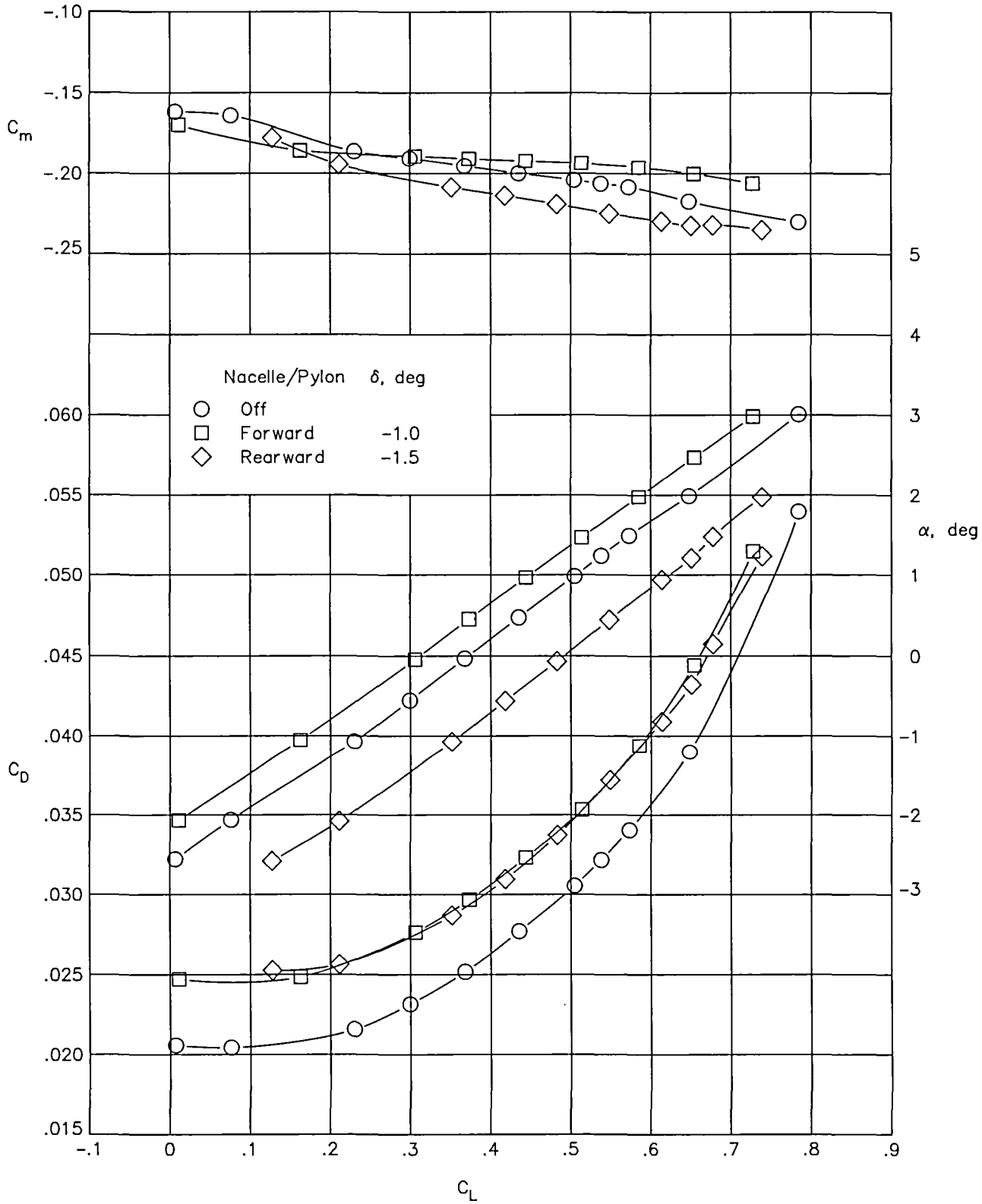

(d) $M = 0.80$.

Figure 7. Continued.

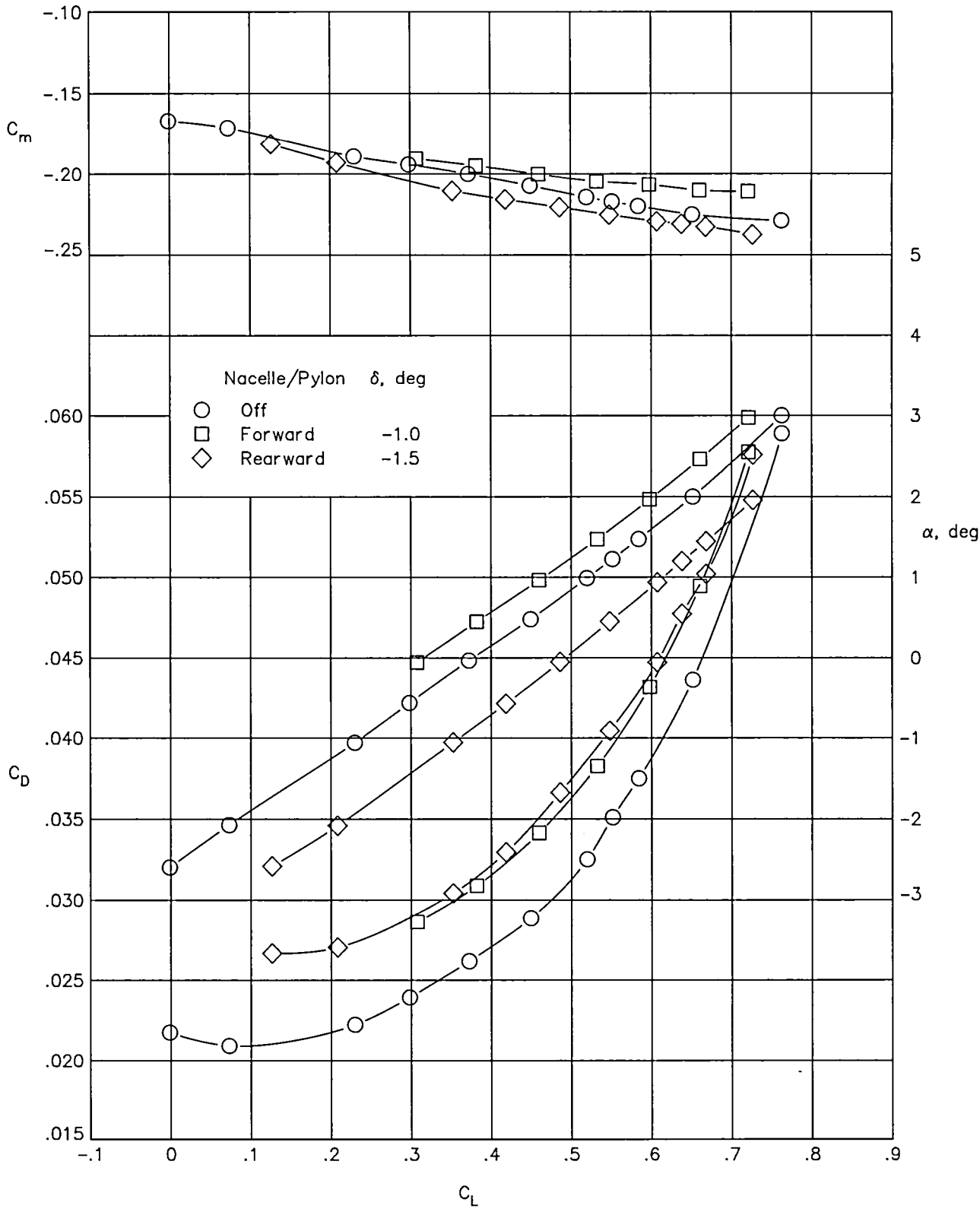

(e) $M = 0.82$.

Figure 7. Concluded.

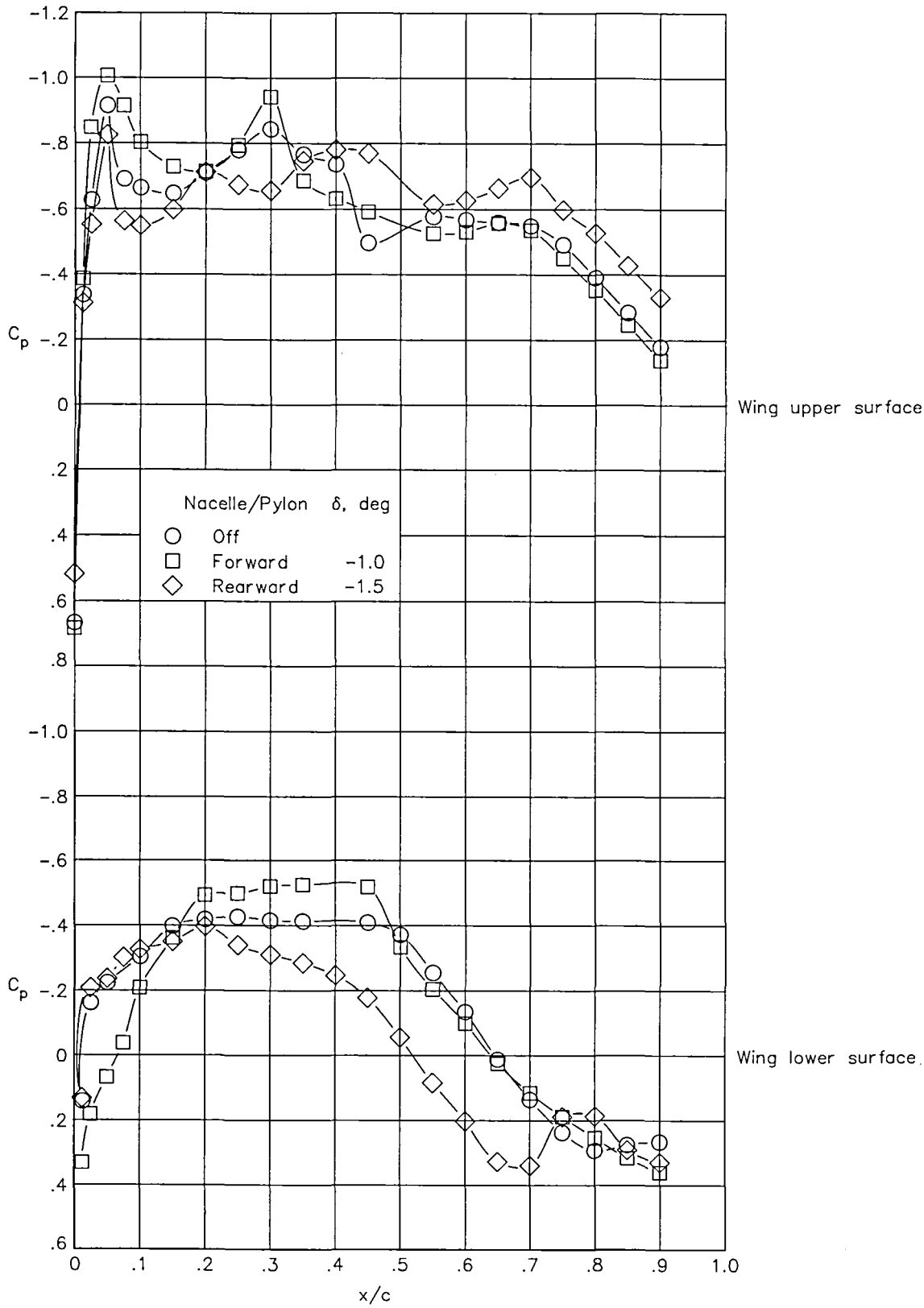

(a) $\eta = 0.328$.

Figure 8. Effects of nacelle/pylon longitudinal location on wing chordwise pressure distribution at $M = 0.80$ and $C_L \approx 0.43$.

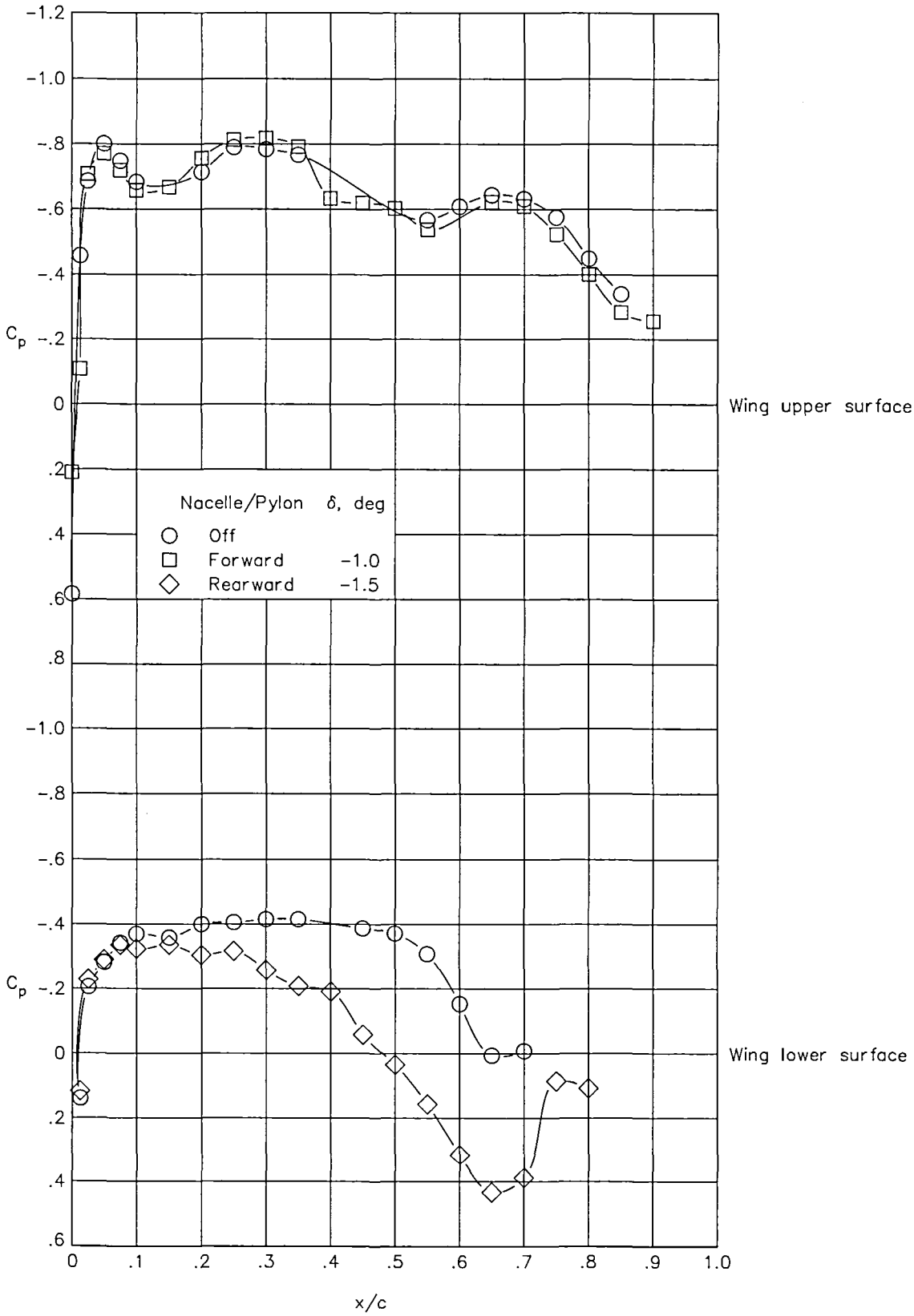

(b) $\eta = 0.370$.

Figure 8. Continued.

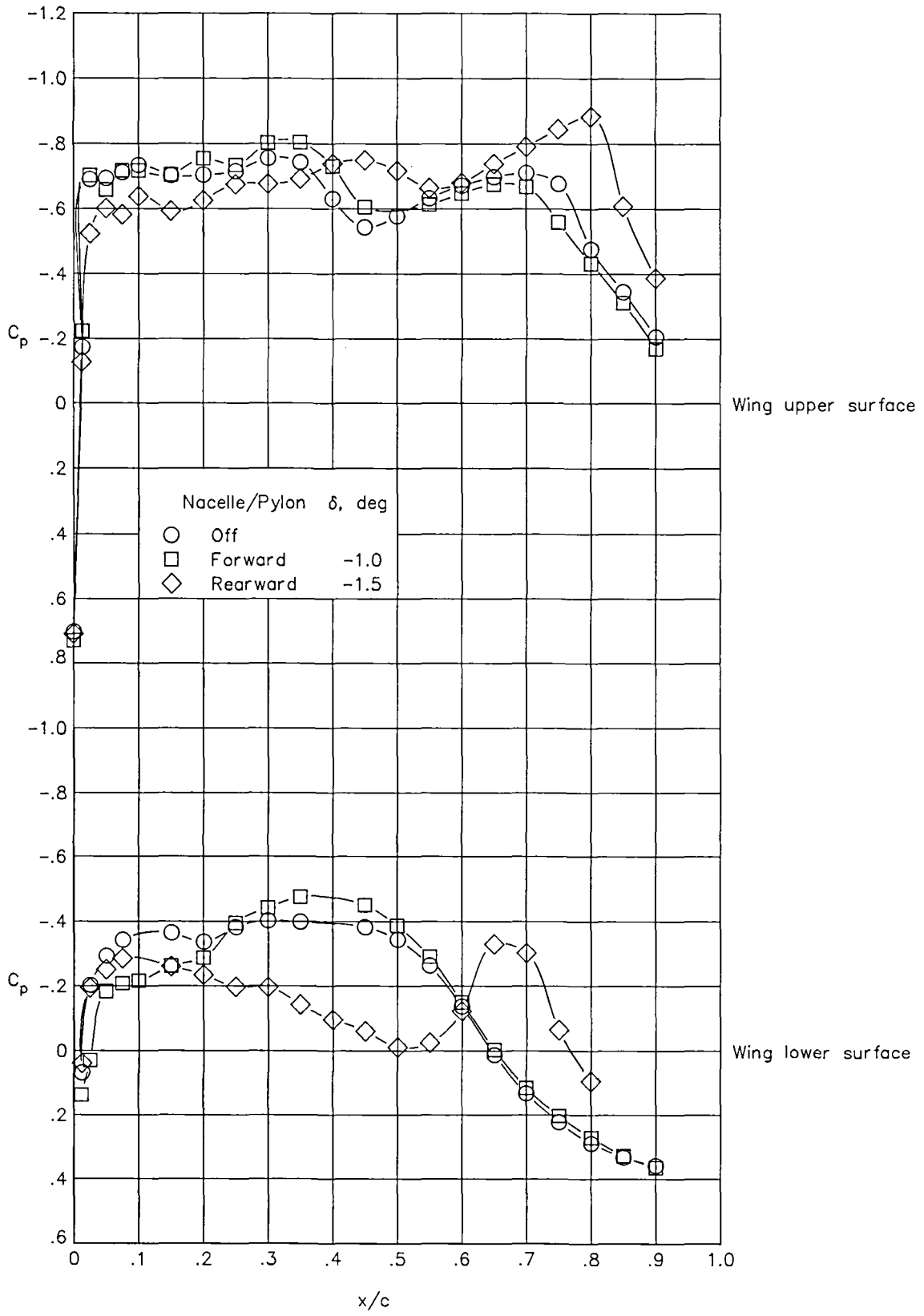

(c) $\eta = 0.440$.

Figure 8. Concluded.

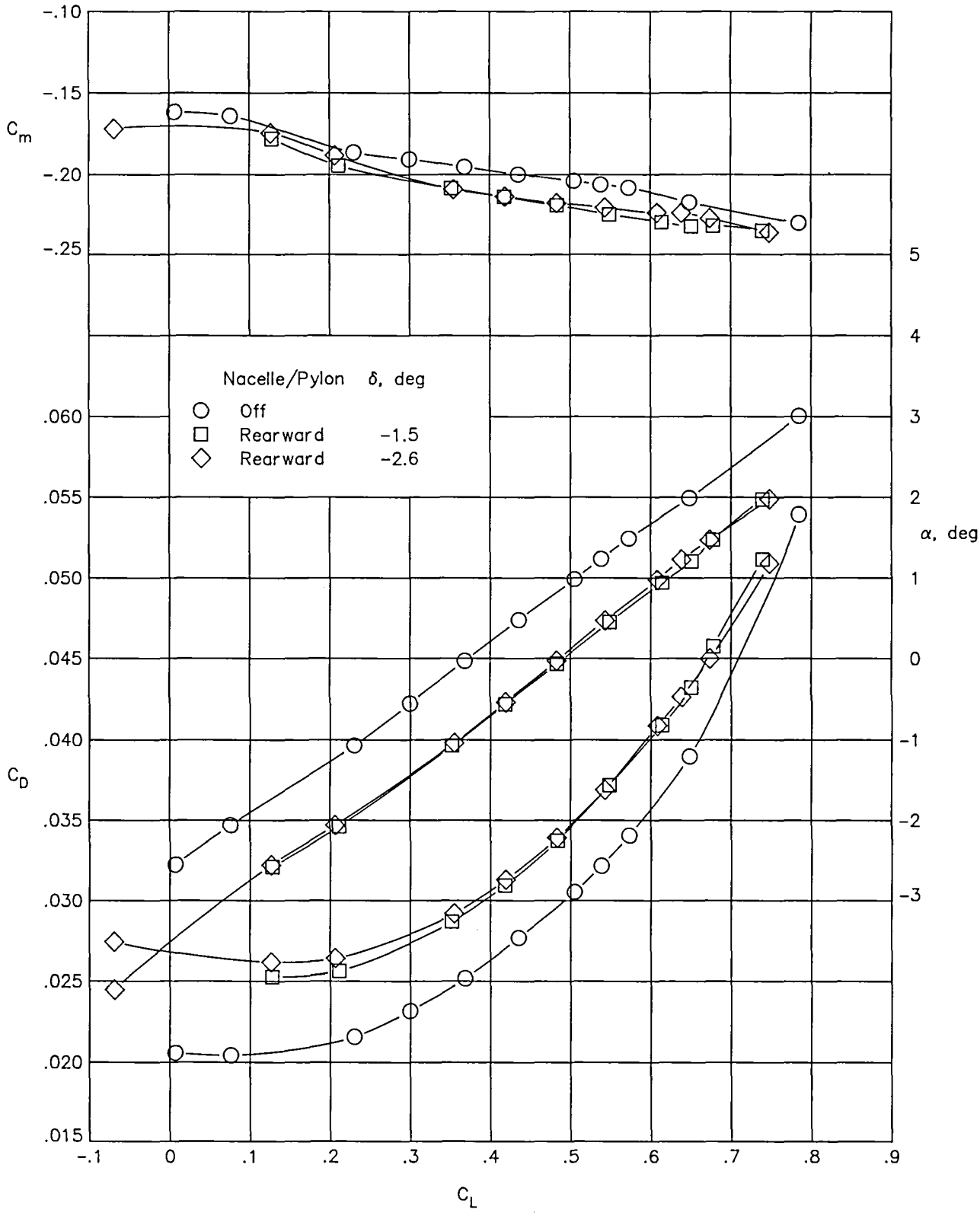

Figure 9. Effects of nacelle/pylon toe-in angle on longitudinal aerodynamic characteristics at $M = 0.80$.

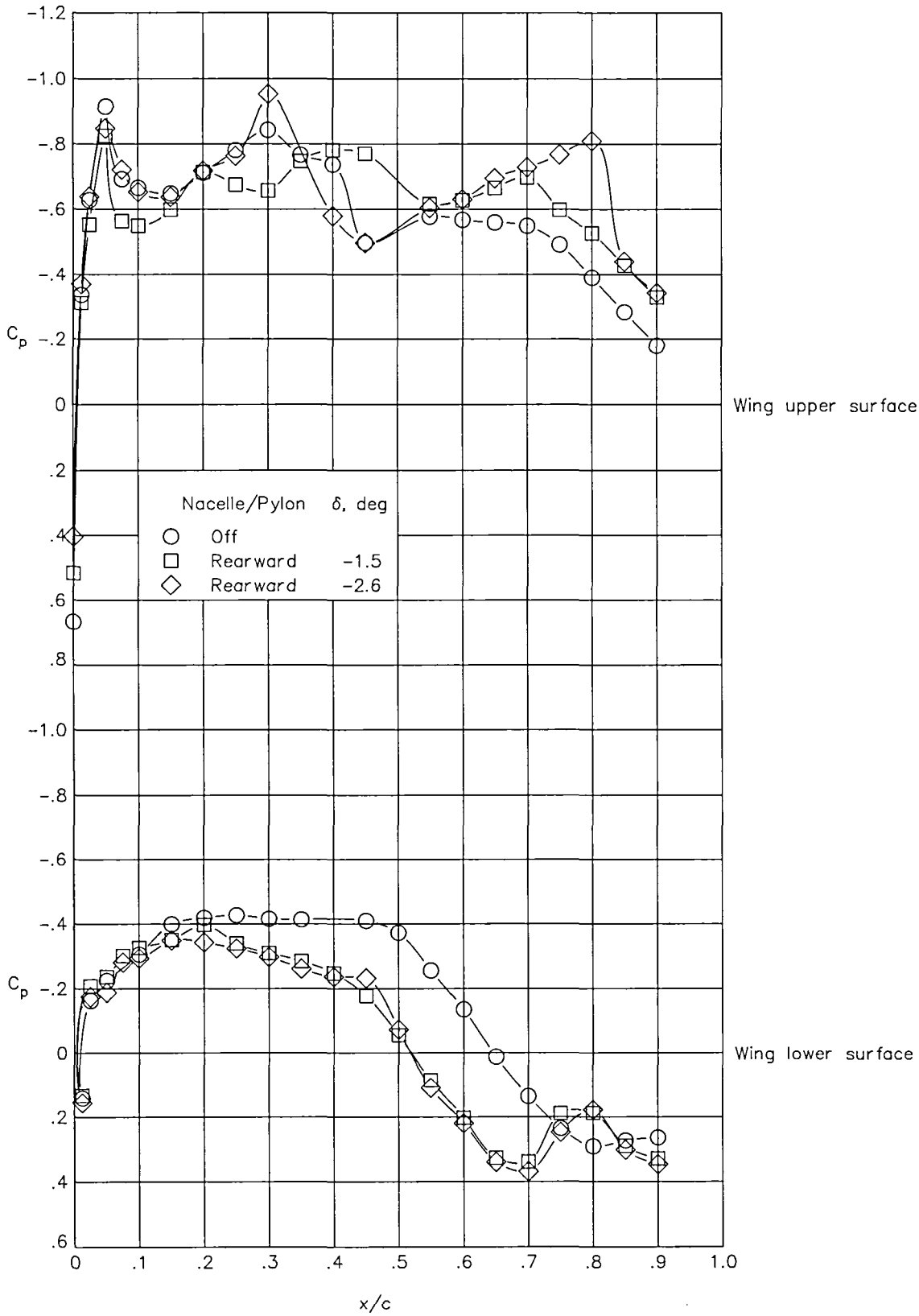

(a) $\eta = 0.328$.

Figure 10. Effects of nacelle/pylon toe-in angle on wing chordwise pressure distribution at $M = 0.80$ and $C_L \approx 0.43$.

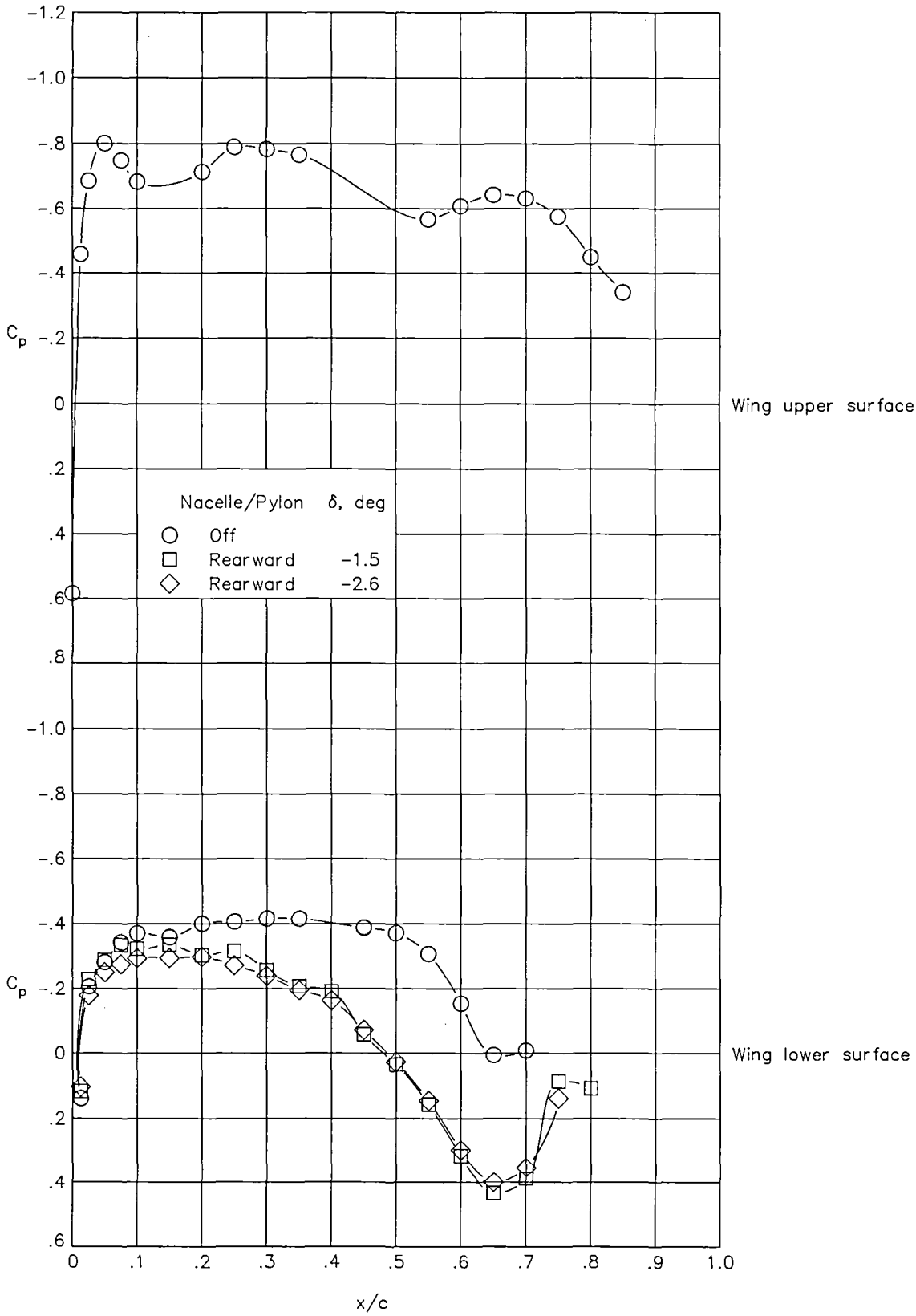

(b) $\eta = 0.370$.

Figure 10. Continued.

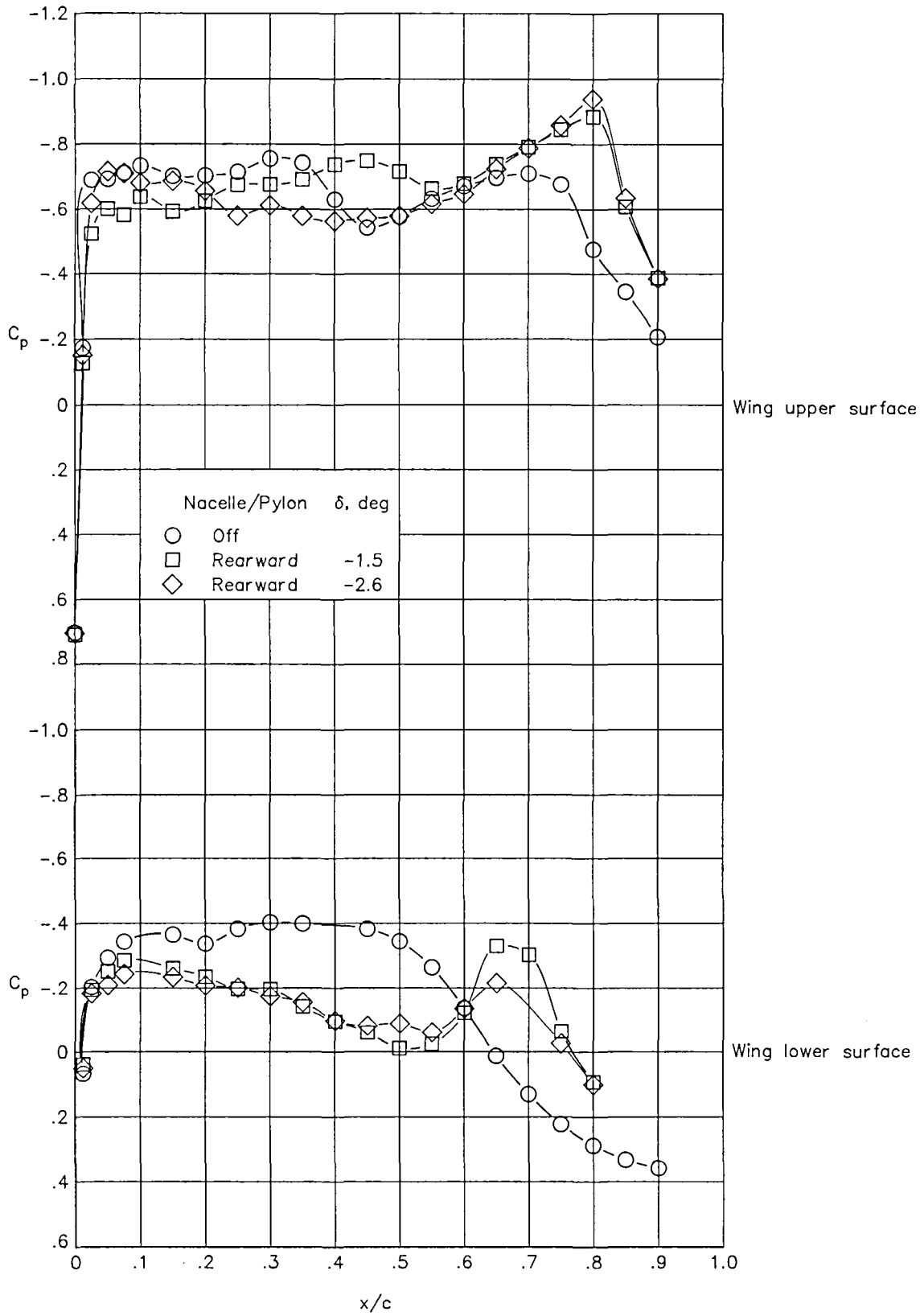

(c) $\eta = 0.440$.

Figure 10. Concluded.

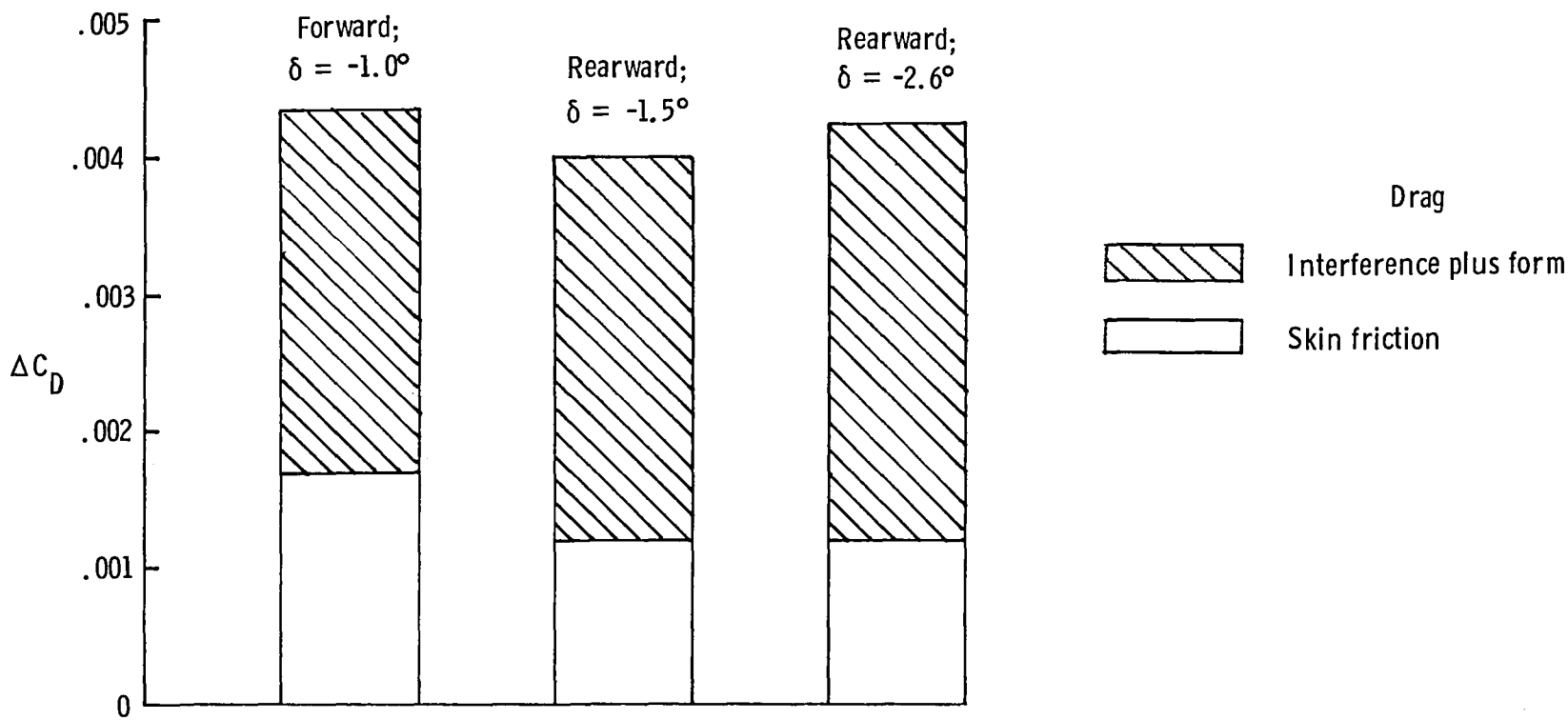

Figure 11. Installed drag coefficient of nacelle/pylon at $M = 0.80$ and $C_L = 0.45$.

1. Report No.	2. Government Accession No.	3. Recipient's Catalog No.
NASA TM-87627		

4. Title and Subtitle	5. Report Date
Integration Effects of Underwing Forward- and Rearward-Mounted Separate-Flow, Flow-Through Nacelles on a High-Wing Transport	April 1986
	6. Performing Organization Code 505-43-90-07
7. Author(s) Milton Lamb and William K. Abeyounis	8. Performing Organization Report No. L-16026
9. Performing Organization Name and Address NASA Langley Research Center Hampton, VA 23665-5225	10. Work Unit No.
	11. Contract or Grant No.
12. Sponsoring Agency Name and Address National Aeronautics and Space Administration Washington, DC 20546-0001	13. Type of Report and Period Covered Technical Memorandum
	14. Sponsoring Agency Code

15. Supplementary Notes

16. Abstract

An experimental investigation has been conducted in the Langley 16-Foot Transonic Tunnel at free-stream Mach numbers from 0.70 to 0.82 and angles of attack from $-2.5°$ to $4.0°$ to determine the integration effects of pylon-mounted underwing forward and rearward separate-flow, flow-through nacelles on a high-wing transonic transport configuration. The results of the investigation showed that the installed drag of the nacelle/pylon in the rearward location was slightly less than that of the nacelle/pylon in the forward location. This reduction was due to the reduction in calculated skin friction of the nacelle/pylon configuration. In all cases the combined value of form, wave, and interference drag was excessively high. However, the configuration with the nacelle/pylon in a rearward location produced an increase in lift over that of the basic wing-body configuration.

17. Key Words (Suggested by Authors(s))	18. Distribution Statement
Nacelle/pylon wing integration Transonic transport Separate-flow, flow-through nacelles Forward- and rearward-mounted nacelles	Unclassified—Unlimited Subject Category 02

19. Security Classif.(of this report)	20. Security Classif.(of this page)	21. No. of Pages	22. Price
Unclassified	Unclassified	28	A03

For sale by the National Technical Information Service, Springfield, Virginia 22161

NASA-Langley, 1986

National Aeronautics and
Space Administration
Code NIT-4

Washington, D.C.
20546-0001

Official Business
Penalty for Private Use, $300

BULK RATE
POSTAGE & FEES PAID
NASA
Permit No. G-27

NASA

POSTMASTER: If Undeliverable (Section 158 Postal Manual) Do Not Return